COMMUNICATION

Novel amphiphilic corannulene additive for moisture-resistant perovskite solar cells

Received 00th January 20xx,
Accepted 00th January 20xx

DOI: 10.1039/x0xx00000x

Bening Tirta Muhammad,[abc] Viktor Barat,[d] Koh Teck Ming,[a] Xihu Wu,[c] Abhijith Surendran,[c] Natalia Yantara,[a] Annalisa Bruno,[a] Andrew C. Grimsdale,[e] Mihaiela C. Stuparu*[de] and Wei Lin Leong*[ac]

The addition of amphiphilic triethylene glycol based corannulene molecule provides multiple Lewis basic sites that assists in perovskite grain growth, improves charge carrier collection and moisture resistance of perovskite solar cells. This study paves ways to utilize more molecules from corannulene families in perovskite research.

Hybrid organic-inorganic perovskite (HOIP) materials have gained huge attention in the new generation photovoltaic research, primarily due to their remarkable photovoltaic performance and low cost large area fabrication potential.[1,2] The power conversion efficiency (PCE) has increased more than six-fold since the initial report of perovskite solar cell (PSC) with a humble PCE of 3.9% in 2009.[3,4] The major development of PSCs in the last decade was attributed to understanding the chemistry of perovskite layer formation, defect engineering and transport layer modifications.[5–8] Despite great achievements in device efficiency, moisture-induced degradation still remains road-blocking to the wide application of PSCs.[9] Several types of organic molecules have been used to increase the hydrophobicity of the perovskite layer. For instances, hydrophobic molecules such as functionalized aliphatic compounds, fullerenes, and ionic liquids were reported to increase moisture-resistance of PSCs when used as additive in perovskite precursor solution.[10–12] Separately, hydrophilic polymers such as poly(ethylene glycol) and poly(acrylic acid) were found to maintain device stability despite their water-absorbing nature.[13,14] However, the beneficial effect of amphiphilic organic molecules has been scarcely discussed. Herein, novel amphiphilic corannulene-pentakis-(triethyleneglycol-monomethyl ether)-sulfone (Cor-TEG) was utilized to explore the mutual effect of both hydrophobic corannulene and hydrophilic side chains (ethylene glycol oligomers) to increase moisture resistance of PSCs. It is found that the Cor-TEG additive modulated the perovskite crystal growth to form large and columnar grains with reduced defects and enhanced photocarrier extraction. Notably, the highest PCE of 17.0% has been attained with Cor-TEG modified perovskite device with improved stability in both inert (91% of initial PCE for 65 days) and humid conditions (87% of initial PCE for two weeks).

Corannulene is a non-planar π-system which can be synthesized at kilogram-scale.[15] It also has high solubility in various common organic solvents used in solution-processed PSC fabrication and can be functionalized in a controlled manner to modulate the electronic properties of the core carbon scaffold.[16] The synthesis of Cor-TEG was carried out by oxidation of the previously reported corannulene-penta(TEG)-sulfide.[17] Using an excess amount of *meta*-chloroperoxybenzoic acid (*m*-CPBA) as the oxidant in dichloromethane (DCM), the reaction was completed within 3 days, and the desired product was purified by a combination of extraction and silica gel chromatography. The obtained Cor-TEG was an orange oil that showed excellent solubility in polar organic solvents such as *N,N*-dimethylformamide (DMF), DCM, chloroform and ethyl acetate. The electron-withdrawing capability of resulting corannulene compound is significantly enhanced by addition of five sulfonyls known as strong electron withdrawing functional groups.[18] In this study, Cor-TEG was added into perovskite precursor solution and stirred for at least one hour. The complete perovskite device fabrication steps can be found in the Experimental Section and the chemical structure of Cor-TEG is shown in Fig. 1a.

The role of Cor-TEG additive was studied in planar perovskite solar cell (PSC) devices. The device architecture of planar PSCs is depicted in Fig. 1b. The current density–voltage (*J*–V) characterizations measured under simulated AM 1.5 radiation of our best cells with and without the Cor-TEG

[a] *Energy Research Institute@NTU (ERI@N), Research Techno Plaza, X-Frontier Block, Level 5, 50 Nanyang Drive, 637553, Singapore*
[b] *Interdisciplinary Graduate Programme, Nanyang Technological University, 639798, Singapore*
[c] *School of Electrical and Electronic Engineering, Nanyang Technological University, 639798, Singapore. Email: wlleong@ntu.edu.sg*
[d] *Division of Chemistry and Biological Chemistry, School of Physical and Mathematical Sciences, Nanyang Technological University, 637371, Singapore. Email: mstuparu@ntu.edu.sg*
[e] *School of Materials Science and Engineering, Nanyang Technological University, 639798, Singapore*
† Electronic Supplementary Information (ESI) available: Experimental details, Fig. S1-S11 and Table S1-S2. See DOI: 10.1039/x0xx00000x

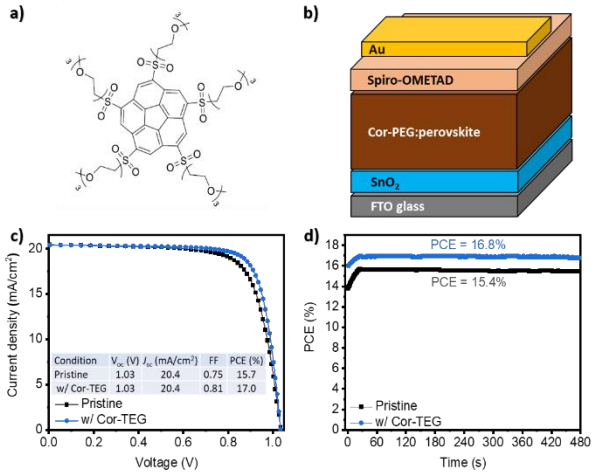

Fig. 1 a) Molecular structure of Cor-TEG molecule. b) Device schematic of planar PSC used in this study, c) *J*-V scan of pristine and Cor-TEG treated devices, and d) stabilized power output tracking under one-sun illumination measured at 0.84 V and 0.87 for pristine and Cor-TEG treated devices, respectively.

additives in the perovskite light absorbers are shown in Figure 1c.

The average device parameters are presented in Table S1. A high PCE of 17% can be achieved for the Cor-TEG treated device. Notably, higher fill factor was observed as predominant factor in the overall increase of device performance. Fig. 1d presents the stabilized power output (SPO) obtained using maximum power point tracking, where the Cor-TEG treated device could still maintain the device efficiency above 16% after 3000 seconds (see Fig. S1) while the pristine one partially degraded in which power output was reduced from 15.4% to 14.1%.

Cor-TEG has 25 oxygen atoms including those of 5 sulfone (O=S=O) functional groups each molecule as the side chains which act as Lewis bases that coordinate to Lewis acidic Pb (II) in perovskite precursor solution, thus slowing down the crystallization process.[19] Interaction between Lewis base sites of Cor-TEG with Pb (II) was confirmed by Fourier Transform Infrared (FTIR) spectroscopy. Several peaks shift to lower wavenumbers were observed, implying efficient coordination with Pb (II).[20,21] Interaction between Lewis base sites of Cor-TEG with Pb (II) was confirmed by Fourier Transform Infrared (FTIR) spectroscopy. Several peaks shift to lower wavenumbers were observed, implying efficient coordination with Pb (II).[20,21] For instances, S=O stretching peak of sulfone and C-O stretching peak of triethyleneglycol (TEG) were red-shifted from 1128 to 1104 cm^{-1} and 1025 to 1019 cm^{-1}, respectively (see Fig. S2). Top-view scanning electron microscopy (SEM) has been utilized to obtain the morphologies for the perovskite films with different amount of Cor-TEG (Fig. 2a-d). The grain size of pristine perovskite was observed to be around 281 nm. Upon addition of Cor-TEG from 4, 10, and 30 µg/mL, the size of perovskite grains increased to 316, 358, and 399 nm, respectively (see also Fig. S3). More compact and smoother perovskite surfaces are also observed which was further confirmed by atomic force microscopy (AFM), where the surface roughness analysis exhibited a reduced root-mean square (RMS) roughness, from 22.0 nm to 18.7 nm for pristine and Cor-TEG treated samples, respectively (Fig. S4). The cross-sectional SEM images (Fig. 2e-h) agree with the larger grain size and clearly illustrate more uniform and columnar perovskite films. This controlled growth of perovskite crystallites is attributed to the role of Lewis bases to the ripening process of perovskite film growth.[22]

Moreover, more columnar-like grains significantly reduce the amount of grain boundaries that are susceptible to degradation reaction in the presence of moisture, which later contribute to the stability of resulting device in ambient conditions.[23,24] However, the x-ray diffraction spectra do not show significant difference in peaks positions and intensity (Fig. S5). We postulate this is likely due to the hydrophilic nature of underlying UV-ozone treated SnO_2 layer that induces large number of nucleation sites at the initial stage of perovskite formation. Overall, increasing amount of Cor-TEG amount directed to beneficial perovskite morphology and grain growth.

The photophysical properties of obtained pristine and modified perovskite films are analyzed by photoluminescence (PL) profiles. Fig. 3a shows that higher intensity of steady-state PL for modified perovskite film and thus correlates well with the improved perovskite film quality. The effect of Cor-TEG addition was further probed through time-resolved PL decay measurement (Fig. 3b). The PL decay curves were fitted by bi-exponential decay function to extract the fast (τ_1) and slow (τ_2) characteristic decay times. The τ_1 and τ_2 are attributed to the non-radiative and radiative recombination of excited charge carrier. Higher value of time constants (slower decay) for Cor-TEG treated perovskite films as compared to the pristine one indicates suppressed amounts of defects and non-radiative recombination which can be further attributed to reduced grain boundaries in the perovskite films.[25] The PL lifetime (τ_{ave}) (see

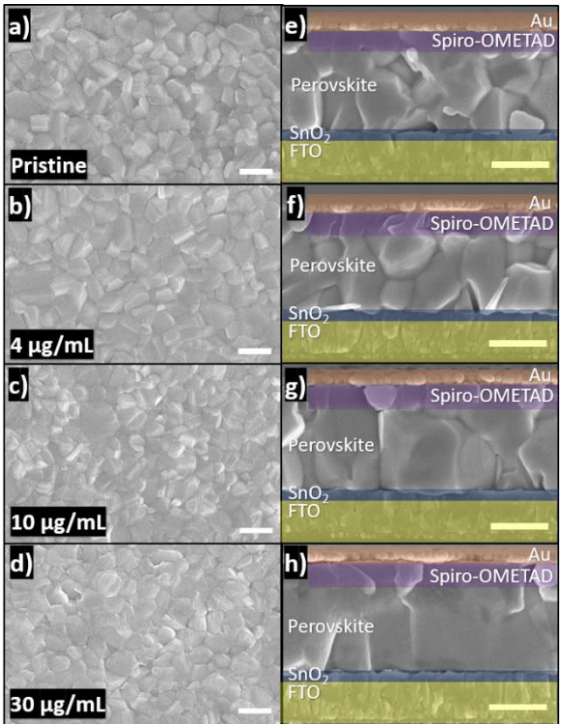

Fig. 2 Top-view SEM images of perovskite films (a-d) and cross-sectional SEM images of pristine and Cor-TEG treated devices (e-h), showing a trend of larger and more columnar grains of perovskite active layer over increasing amount of Cor-TEG. Statistical presentation of grain sizes is presented in Fig. S3. Scale bars are of 500 nm.

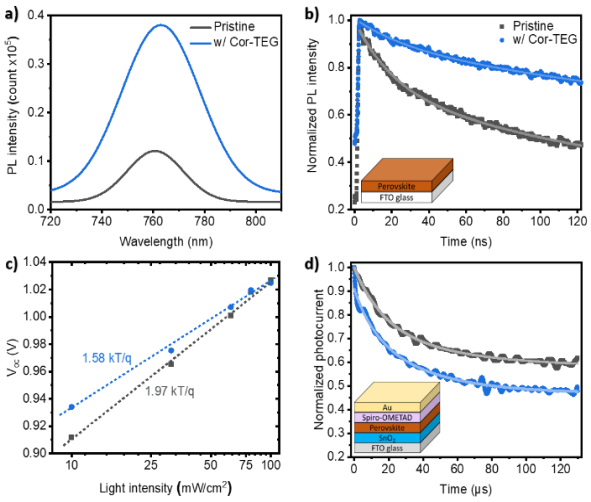

Fig. 3 a-b) steady-state and time-resolved photoluminescence (PL) profiles of pristine and Cor-TEG treated perovskite films on glass substrate, c) light intensity-dependent open-circuit voltage measurement and d) photo-current decay profile of complete devices for pristine and Cor-TEG treated conditions.

Table S2) has been evaluated from the amplitude weighted average of the two characteristic lifetimes times. The addition of Cor-TEG also significantly prolongs the PL τ_{ave} from 157 ns to 454 ns.

Figure 3c depicts the light intensity dependence of open-circuit voltages (V_{oc}) for the devices. It has been shown that the recombination modes is related to the ideality factor (n) of the device and is extracted through the slope of nkT/q in the semi-logarithmic plot of V_{oc} versus light intensity (q is the elementary charge, *T* is temperature in Kelvin, *k* is Boltzmann constant). When n=1, the dominant loss mechanism is band-to-band recombination while n=2 refers to trap-assisted recombination.[26] Under the light irradiance range of 10 mW/cm^2 to 100 mW/cm^2 (1-sun) irradiance, the Cor-TEG modified devices exhibit lower ideality factor than that of pristine ones, i.e. 1.58 and 1.97, respectively. This measurement suggests the reduced defect states from perovskite films upon utilization of Cor-TEG as additive which correlates well with the larger grain size and reduced grain boundaries as observed in the SEM. The reduced defect states were also reflected in the smaller hysteresis between reverse and forward scans of *J*-V curve (Fig. S6). Moreover, the smoother perovskite surface as seen in AFM images (Fig. S4) could result in a more conformal packing of hole-transport layer (HTL) on top of the perovskite layer, giving rise to the improved interface in working device. The electron withdrawing nature of sulfone-functionalized corannulene could also play an important role in bridging inter-grain charge transport, facilitating the photocurrent extraction as shown in Fig. 3d. The charge carrier property was analyzed by probing the photocurrent decay after perturbation with small increase in light intensity. This method elucidates the kinetic of carrier extraction upon light illumination. Therefore, a faster decay was observed on Cor-TEG treated device (17.0 μs) than the pristine one (21.2 μs) following an exponential decay fitting to obtained photocurrent signals. This finding is in good agreement with hypothesized role of Cor-TEG at bridging intra-grain transport utilizing the electron withdrawing nature of the electron-poor polyaromatic core.

The stability test of the devices has been completed during a period of 65 days and the results are shown in Fig. 4a. The devices are stored in argon-filled glovebox. As compared to pristine device that could only retain 61% of its initial PCE, the Cor-TEG modified perovskite solar cell can hold ~91% of its initial PCE. Ambient stability of obtained PSCs was also tracked over the course of 2 weeks. These devices were not encapsulated and exposed to ambient atmosphere with measured relative humidity of 70%. The Cor-TEG treated devices demonstrated excellent stability and retained 87% of their initial efficiency in such harsh environment (Fig. 4b). The major factors of performance decrease over the time appeared to be the degraded perovskite active layer and deteriorated interface as seen in lower J_{sc} and FF, respectively (Fig. S7). The moisture stability of Cor-TEG treated device was then traced from the stability of the perovskite layer. X-ray diffraction spectra of fresh and aged perovskite films of pristine and Cor-TEG modified conditions are presented in Fig. 4c and 4d. There are two peaks clearly indicating severe degradation in pristine films. First, the peak at 12.7° is known to hint relative amount of lead iodide, the by-product of perovskite degradation reaction. Second, the peak at lower angle ca. 11.3° could be attributed to perovskite monohydrate species[23] with respect to moisture-induced degradation mechanism predominant when perovskite film is exposed in high humidity atmosphere. The quantification on relative intensities from respective peaks indicate that in pristine sample, after storing for 8 days in a controlled chamber with 50% RH, 73% perovskite had degraded, referring to strong perovskite monohydrate and PbI_2 peaks at 11.3° and 12.7°, respectively. Remarkably, only a

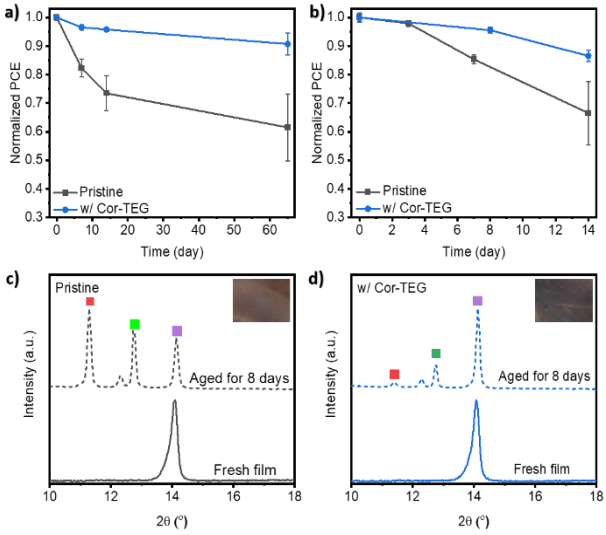

Fig. 4 Stability tracking for four devices upon (a) storage in argon-filled glovebox over 65 days and b) humidity stress at 70% relative humidity over 2 weeks and. Note that all *J*-V measurements were carried out in ambient atmosphere. c-d) X-ray diffraction spectra of pristine and Cor-TEG treated perovskite films at t = 0 day (fresh) and t = 8 days, the insets are photographs of respective aged films in which that of pristine one appears yellowish. Purple, green and red squares are peaks of perovskite, PbI_2 (degradation by-product), and perovskite monohydrate (degradation intermediate due to moisture adsorption), respectively.

minute intensity is observed at 11.3° for Cor-TEG modified perovskite films which strongly suggests that moisture adsorption and ingress could be inhibited by the presence of Cor-TEG molecules at the peripheral of crystal grains. Moreover, the presence of Cor-TEG on perovskite surface was confirmed by water droplet contact angle measurement whereas Cor-TEG treated perovskite film exhibits slightly higher angle (Fig. S8) which also supports the role of Cor-TEG to protect underlying perovskite layer from the surface. The protection from moisture-induced degradation found in this study was in accordance to previous reports whereby long chains of poly(ethylene glycol)-functionalized additive were used in both perovskite precursor[27] and anti-solvent mixture[28]. Here, the ambient stability is thus attributed to TEG chains present in the Cor-TEG molecule. Counter-intuitively, the TEG chains known for the hygroscopicity could prevent degradation by passivating uncoordinated Pb ions on perovskite surface and as well as slow down perovskite hydration process by containing the water molecules before reaching the perovskite layer.[20]

In summary, we have shown that TEG-sulfone substituted corannulene (Cor-TEG) additive serve to improve perovskite film morphology with larger grain size and columnar-like and enhance the interfacial quality as shown by higher fill factor of 81% and overall decent efficiency of 17%. Moreover, the improved charge extraction, as shown in photocurrent decay curves, was attributed to the electron withdrawing nature of corannulene sulfone. The enhanced moisture resistance was attributed to the protective role of TEG chains in Cor-TEG. Overall, the benefits of corannulene and TEG chains were combined and proved to be favorable in both device performance and stability. To the best of our knowledge, this work presents the first study of corannulene family into perovskite solar cell research to improve device efficiency and moisture resistance. The methodology in this works is simple and only requires very minute amount of additive, allowing utilization in large area perovskite solar panel fabrication.

This research was supported by NTU start-up grants (M4081866, M4081566), Ministry of Education (MOE) under AcRF Tier 2 grant (2018-T2-1-075), A*STAR AME IAF-ICP Grant (No. I1801E0030), A*STAR AME IRG A1883c0006 and National Research Foundation, Prime Minister's Office, Singapore, under Energy Innovation Research Program and Intra-CREATE collaborative grant (NRF2015EWT-EIRP003-004, NRF2018-ITC001-001 and Solar CRP: S18-1176-SCRP). The authors would like to thank Prof. Subodh Mhaisalkar and Prof. Nripan Mathews for useful discussions and the help of Bhumika Chaudhary for XRD measurements.

Conflicts of interest

There are no conflicts to declare.

Notes and references

1 Y. Rong, Y. Hu, A. Mei, H. Tan, M. I. Saidaminov, S. I. Seok, M. D. McGehee, E. H. Sargent and H. Han, *Science*, 2018, **361**, eaat8235.
2 G. Xing, N. Mathews, S. Sun, S. S. Lim, Y. M. Lam, M. Graʈzel, S. Mhaisalkar and T. C. Sum, *Science*, 2013, **342**, 344–347.
3 A. Kojima, K. Teshima, Y. Shirai and T. Miyasaka, *J. Am. Chem. Soc.*, 2009, **131**, 6050–6051.
4 https://www.nrel.gov/pv/assets/pdfs/best-research-cell-efficiencies.20200406.pdf, accessed on May 28, 2020.
5 M. Saliba, T. Matsui, K. Domanski, J. Y. Seo, A. Ummadisingu, S. M. Zakeeruddin, J. P. Correa-Baena, W. R. Tress, A. Abate, A. Hagfeldt and M. Grätzel, *Science*, 2016, **354**, 206–209.
6 M. Jung, S. G. Ji, G. Kim and S. Il Seok, *Chem. Soc. Rev.*, 2019, **48**, 2011–2038.
7 E. H. Jung, N. J. Jeon, E. Y. Park, C. S. Moon, T. J. Shin, T. Y. Yang, J. H. Noh and J. Seo, *Nature*, 2019, **567**, 511–515.
8 W. S. Yang, B. W. Park, E. H. Jung, N. J. Jeon, Y. C. Kim, D. U. Lee, S. S. Shin, J. Seo, E. K. Kim, J. H. Noh and S. Il Seok, *Science*, 2017, **356**, 1376–1379.
9 C. C. Boyd, R. Cheacharoen, T. Leijtens and M. D. McGehee, *Chem. Rev.*, 2019, **119**, 3418–3451.
10 F. Zhang, W. Shi, J. Luo, N. Pellet, C. Yi, X. Li, X. Zhao, T. J. S. Dennis, X. Li, S. Wang, Y. Xiao, S. M. Zakeeruddin, D. Bi and M. Grätzel, *Adv. Mater.*, 2017, **29**, 1606806.
11 B. Kim, M. Kim, J. H. Lee and S. Il Seok, *Adv. Sci.,* 2019, **7**, 1901840.
12 D. Liu, Z. Shao, J. Gui, M. Chen, M. Liu, G. Cui, S. Pang and Y. Zhou, *Chem. Commun.*, 2019, **55**, 11059–11062.
13 Y. Zhao, J. Wei, H. Li, Y. Yan, W. Zhou, D. Yu and Q. Zhao, *Nat. Commun.*, 2016, **7**, 10228.
14 D. J. Fairfield, H. Sai, A. Narayanan, J. V. Passarelli, M. Chen, J. Palasz, L. C. Palmer, M. R. Wasielewski and S. I. Stupp, *J. Mater. Chem. A*, 2019, **7**, 1687.
15 A. M. Butterfield, B. Gilomen and J. S. Siegel, *Org. Process. Res. Dev.*, 2012, **16**, 664–676.
16 V. Barát, M. Budanović, D. Halilovic, J. Huh, R. D. Webster, S. H. Mahadevegowda and M. C. Stuparu, *Chem. Commun.*, 2019, **55**, 3113.
17 S. H. Mahadevegowda and M. C. Stuparu, *European J. Org. Chem.*, 2017, 570–576.
18 V. Barát, M. Budanovic, S. M. Tam, J. Huh, R. D. Webster and M. C. Stuparu, *Chem. - A Eur. J.*, 2020, **26**, 3231–3235.
19 J. W. Lee, H. S. Kim and N. G. Park, *Acc. Chem. Res.*, 2016, **49**, 311–319.
20 M. Kim, S. G. Motti, R. Sorrentino and A. Petrozza, *Energy Environ. Sci.*, 2018, **11**, 2609–2619.
21 Y. Ren, X. Ding, J. Zhu, T. Hayat, A. Alsaedi, Z. Li, X. Xu, Y. Ding, S. Yang, M. Kong and S. Dai, *J. Alloys Compd.*, 2018, **758**, 171–176.
22 L. Zhu, Y. Xu, P. Zhang, J. Shi, Y. Zhao, H. Zhang, J. Wu, Y. Luo, D. Li and Q. Meng, *J. Mater. Chem. A*, 2017, **5**, 20874,
23 A. M. A. Leguy, Y. Hu, M. Campoy-Quiles, M. I. Alonso, O. J. Weber, P. Azarhoosh, M. Van Schilfgaarde, M. T. Weller, T. Bein, J. Nelson, P. Docampo and P. R. F. Barnes, *Chem. Mater.*, 2015, **27**, 3397–3407.
24 Q. Wang, B. Chen, Y. Liu, Y. Deng, Y. Bai, Q. Dong and J. Huang, *Energy Environ. Sci.*, 2017, **10**, 516.
25 T. S. Sherkar, C. Momblona, L. Gil-Escrig, J. Ávila, M. Sessolo, H. J. Bolink and L. J. A. Koster, *ACS Energy Lett.*, 2017, **2**, 1214–1222.
26 W. Tress, M. Yavari, K. Domanski, P. Yadav, B. Niesen, J. P. Correa Baena, A. Hagfeldt and M. Graetzel, *Energy Environ. Sci.*, 2018, **11**, 151–165.
27 S. Collavini, M. Saliba, W. R. Tress, P. J. Holzhey, S. F. Völker, K. Domanski, S. H. Turren-Cruz, A. Ummadisingu, S. M. Zakeeruddin, A. Hagfeldt, M. Grätzel and J. L. Delgado, *ChemSusChem*, 2018, **11**, 1032–1039.
28 Q. Fu, S. Xiao, X. Tang, Y. Chen and T. Hu, *ACS Appl. Mater. Interfaces*, 2019, **11**, 24782–24788.

